

Complete the Missing Half: Augmenting Aggregation Filtering with Diversification for Graph Convolutional Networks

Sitao Luan^{1,2,*}, Mingde Zhao^{1,2,*}, Chenqing Hua^{1,*}, Xiao-Wen Chang¹, Doina Precup^{1,2,3}
 {sitao.luan@mail, mingde.zhao@mail, chenqing.hua@mail, chang@cs, dprecup@cs}.mcgill.ca
¹McGill University; ²Mila; ³DeepMind
 *Equal Contribution

Abstract

The core operation of current Graph Neural Networks (GNNs) is the *aggregation* enabled by the graph Laplacian or message passing, which filters the neighborhood node information. Though effective for various tasks, in this paper, we show that they are potentially a problematic factor underlying all GNN methods for learning on certain datasets, as they force the node representations similar, making the nodes gradually lose their identity and become indistinguishable. Hence, we augment the aggregation operations with their dual, *i.e.* diversification operators that make the node more distinct and preserve the identity. Such augmentation replaces the aggregation with a two-channel filtering process that, in theory, is beneficial for enriching the node representations. In practice, the proposed two-channel filters can be easily patched on existing GNN methods with diverse training strategies, including spectral and spatial (message passing) methods. In the experiments, we observe desired characteristics of the models and significant performance boost upon the baselines on 9 node classification tasks.

Introduction

As a generic data structure, graph is capable of modeling complex relations among objects in many real-world problems (Liao et al. 2019; Monti et al. 2017; Defferrard, Bresson, and Vandergheynst 2016). Motivated by the success of Convolutional Neural Networks (CNNs) (LeCun et al. 1998) on images, graph convolution (Wu et al. 2019b) is defined on the graph Fourier domain and the node spatial neighborhood domain (Zhang et al. 2019), respectively, in the form of spectral- and spatial-based methods. Based on the 2 methodologies, different (linear) graph filters and (non-linear) deep learning techniques (LeCun, Bengio, and Hinton 2015) are combined, giving rise to Graph Neural Networks (GNNs), achieving remarkable progress (Bruna et al. 2014; Hamilton, Ying, and Leskovec 2017; Gilmer et al. 2017; Kipf and Welling 2016; Velickovic et al. 2017; Luan et al. 2019).

Essentially vertex localization, most existing graph filters can be viewed as operators that aggregate node

information from its direct neighbors. Different graph filters yield different spectral GNNs or spatial aggregation functions. Among them, the most commonly used is the *renormalized Laplacian* (Kipf and Welling 2016). By adding an identity to the adjacency matrix, *i.e.* a self-loop in the graph topology, renormalized graph Laplacian is created as a low-pass (LP) filter (Maehara 2019) mainly capturing low-frequency signals, which are locally smooth features across the whole graph (Wu et al. 2019a). Aggregation processes, in the form of message passing used in spatial-based methods, as in *e.g.*, GraphSAGE (Hamilton, Ying, and Leskovec 2017) and GraphSAINT (Zeng et al. 2019), are also node-level LP filters which make nodes become similar to their neighbors.

The main idea of node aggregation is to exploit the intrinsic geometry of the data distribution: if 2 data points are close (or connected) to each other on the manifold, they should be also close to each other in the representation space. This assumption is usually referred to as manifold (local invariance) (Belkin and Niyogi 2002; He and Niyogi 2004; Cai, Wang, and He 2009; Cai et al. 2010), assortative mixing (assortativity) (Newman 2003), homophily (McPherson, Smith-Lovin, and Cook 2001) or smoothness (Kalofolias 2016) assumption, which play an essential role in the development of various kinds of algorithms including dimensionality reduction (Belkin and Niyogi 2002) and semi-supervised learning (Zhou et al. 2004)¹. This assumption naturally holds in many real world networks (McPherson, Smith-Lovin, and Cook 2001; Jiang, Bolnick, and Kirkpatrick 2013), *e.g.*, social networks, citation networks, evolutionary biology *etc.*. However, in contrast to homophily, there also exists a large number of heterophily networks where individuals with diverse characteristics tend to gather in the same group (Rogers 2010), *e.g.*, dating networks (Zhu et al. 2020) and fraudsters in online purchasing networks (Pandit et al. 2007). On these networks, there is no strong reason to impose smoothness assumption and on the contrary, non-smoothness pattern between nodes turns out to be

¹In this paper, we do not distinguish the name of this assumption.

important.

With the above in mind, in this paper we first propose a method to measure the smoothness of the input features and output labels of an attribute graph based on Dirichlet energy and graph signal energy. With the proposed method, we measure the smoothness of 9 real world datasets, which shows that signal defined on graph is generally a mixture of smooth and non-smooth graph signals and each part plays an indispensable role. Motivated by this discovery, we argue that, to learn richer representations, the distinctive information between nodes should also be extracted. Hence, we design a two-channel filterbank (FB) (Ekambaram 2014) GNN framework which use low-pass (LP) and high-pass (HP) filters to learn the smooth and non-smooth components, respectively. FB-GNN framework can easily be plugged into spatial methods, with LP filter for aggregation operation and HP filter for diversification operation. With experiments on 9 real world datasets, we find that the the HP channel indeed plays an important role in the representation learning, and one-channel baseline methods can gain significant performance boost after being augmented by two-channel methods.

Preliminaries

After introducing the prerequisites, in this section, we formalize the idea behind graph signal filtering. We use bold fonts for vectors (e.g., v), block vectors (e.g., V) and matrix blocks (e.g., V_i). Suppose we have an undirected connected graph $\mathcal{G} = (\mathcal{V}, \mathcal{E}, A)$ without bipartite component, where \mathcal{V} is the node set with $|\mathcal{V}| = N$, \mathcal{E} is the edge set, $A \in \mathbb{R}^{N \times N}$ is a symmetric adjacency matrix with $A_{ij} = 1$ if and only if $e_{ij} \in \mathcal{E}$ otherwise $A_{ij} = 0$, D is the diagonal degree matrix, i.e. $D_{ii} = \sum_j A_{ij}$ and $\mathcal{N}_i = \{j : e_{ij} \in \mathcal{E}\}$ is the neighborhood set of node i . A graph signal is a vector $x \in \mathbb{R}^N$ defined on \mathcal{V} , where x_i is defined on the node i . We also have a feature matrix $X \in \mathbb{R}^{N \times F}$ whose columns are graph signals and each node i has a feature vector $X_{i,:}$ with dimension F , which is the i -th row of X .

Graph Laplacian and Affinity Matrix

The (Combinatorial) graph Laplacian is defined as $L = D - A$, which is a Symmetric Positive Semi-Definite (SPSD) matrix (Chung and Graham 1997). Its eigendecomposition gives $L = U\Lambda U^T$, where the columns of $U \in \mathbb{R}^{N \times N}$ are orthonormal eigenvectors, namely the graph Fourier basis, $\Lambda = \text{diag}(\lambda_1, \dots, \lambda_N)$ with $\lambda_1 \leq \dots \leq \lambda_N$ and these eigenvalues are also called frequencies. The graph Fourier transform of the graph signal x is defined as $x_{\mathcal{F}} = U^{-1}x = U^T x = [u_1^T x, \dots, u_N^T x]^T$, where $u_i^T x$ is the component of x in the direction of u_i .

A smaller λ_i indicates a smoother basis function u_i defined on \mathcal{G} (Daković, Stanković, and Sejdić 2019), which means any two elements of u_i corresponding to two connected nodes will have more similar values. This is because finding the eigenvalues and eigen-

vectors of graph Laplacian is actually solving a series of conditioned minimization problems relevant to the smoothness of the function defined on \mathcal{G} .

Some variants of graph Laplacians are commonly used in practice, e.g., the symmetric normalized Laplacian $L_{\text{sym}} = D^{-1/2}LD^{-1/2} = I - D^{-1/2}AD^{-1/2}$, the random walk normalized Laplacian $L_{\text{rw}} = D^{-1}L = I - D^{-1}A$. L_{rw} and L_{sym} share the same eigenvalues, which are inside $[0, 2)$, and their corresponding eigenvectors satisfy $u_{\text{rw}}^i = D^{-1/2}u_{\text{sym}}^i$.

The affinity (transition) matrix derived from L_{rw} is defined as $A_{\text{rw}} = I - L_{\text{rw}} = D^{-1}A$ and its eigenvalues $\lambda_i(A_{\text{rw}}) = 1 - \lambda_i(L_{\text{rw}}) \in (-1, 1]$. Similarly, $A_{\text{sym}} = I - L_{\text{sym}} = D^{-1/2}AD^{-1/2}$ is an affinity matrix as well. Renormalized affinity matrix is introduced in (Kipf and Welling 2016) and defined as $\hat{A}_{\text{rw}} = \tilde{D}^{-1}\tilde{A}$, where $\tilde{A} \equiv A + I$, $\tilde{D} \equiv D + I$ and $\lambda(\hat{A}_{\text{rw}}) \in (-1, 1]$. It essentially defines a random walk matrix on \mathcal{G} with a self-loop added to each node in \mathcal{V} and is widely used in GCN as follows,

$$Y = \text{softmax}(\hat{A}_{\text{rw}} \text{ReLU}(\hat{A}_{\text{rw}} X W_0) W_1) \quad (1)$$

where $W_0 \in \mathbb{R}^{F \times F_1}$ and $W_1 \in \mathbb{R}^{F_1 \times O}$ are parameter matrices. \hat{L}_{rw} can be defined as $I - \hat{A}_{\text{rw}}$. $\hat{A}_{\text{sym}} \equiv \tilde{D}^{-1/2}\tilde{A}\tilde{D}^{-1/2}$ can also be applied in GCN and $\hat{L}_{\text{sym}} = I - \hat{A}_{\text{sym}}$. Specifically, the nature of transition matrix makes \hat{A}_{rw} behave as a mean aggregator $(\hat{A}_{\text{rw}}x)_i = \sum_{j \in \{\mathcal{N}_i \cup i\}} x_j / (D_{ii} + 1)$ which is applied in (Hamilton, Ying, and Leskovec 2017) and is important to bridge the gap between spatial- and spectral-based graph convolution methods.

Measure of Smoothness and (Dirichlet) Energy

Dirichlet Energy is often used to measure how variable a function is (Evans 1998) and for signal defined on graph, it can measure the global smoothness of the signal (Shuman et al. 2013; Bronstein et al. 2016; Smith, Spyrou, and Escudero 2018) and is defined as follows.

Definition 1. (Dirichlet Energy) The Dirichlet energy of block matrix X and column vector x defined on \mathcal{G} are separately defined as

$$E_S^{\mathcal{G}}(X) = \text{tr}(X^T L X), \quad E_S^{\mathcal{G}}(x) = x^T L x \quad (2)$$

Note that $E_S^{\mathcal{G}}$ is always non-negative since L is SPSPD. The graph signal energy is defined as follows.

Definition 2. (Graph Signal Energy (Gavili and Zhang 2017; Stanković, Sejdić, and Daković 2018)) The signal energy of block matrix X and column vector x defined on undirected graph \mathcal{G} are separately defined as

$$E^{\mathcal{G}}(X) = \text{tr}(X^T X), \quad E^{\mathcal{G}}(x) = x^T x \quad (3)$$

The signal energy represents the amount of contents in a graph signal and we will draw the correlation between $E_S^{\mathcal{G}}$ and $E^{\mathcal{G}}$ and explain how they can be used

to measure the smoothness and non-smoothness of a graph (block) signal.

Take column vector \mathbf{x} for example, $E_S^{\mathcal{G}}(\mathbf{x})$ can be written as,

$$\mathbf{x}^T L \mathbf{x} = \sum_i \lambda_i (u_i^T \mathbf{x})^T u_i^T \mathbf{x} = \sum_i \lambda_i \|u_i^T \mathbf{x}\|_2^2$$

The frequency λ_i before $\|u_i^T \mathbf{x}\|_2^2$ can be considered as a weight and $E_S^{\mathcal{G}}(\mathbf{x})$ focuses on measuring the component of \mathbf{x} in the direction of non-smooth u_i , who has a large weight λ_i . A small $E_S^{\mathcal{G}}(\mathbf{x})$ means \mathbf{x} does not contain much non-smooth components. $E^{\mathcal{G}}(\mathbf{x})$ can be written as

$$\mathbf{x}^T \mathbf{x} = \sum_i (u_i^T \mathbf{x})^T u_i^T \mathbf{x} = \sum_i \|u_i^T \mathbf{x}\|_2^2$$

Signal \mathbf{x} can be decomposed into smooth and non-smooth components, and the amount the non-smooth component can be measured by

$$E_{NS}^{\mathcal{G}}(\mathbf{x}) = E^{\mathcal{G}}(\mathbf{x}) - E_S^{\mathcal{G}}(\mathbf{x}) = \mathbf{x}^T (I - L) \mathbf{x} = \sum_i (1 - \lambda_i) \|u_i^T \mathbf{x}\|_2^2$$

Note that $E_{NS}^{\mathcal{G}}(\mathbf{x})$ can be negative and a small $E_{NS}^{\mathcal{G}}(\mathbf{x})$ indicates that \mathbf{x} is highly non-smooth.

Upon the above analysis, we define $S(\mathbf{x})$ to measure the smoothness of a signal as follows

$$S(\mathbf{x}) = \frac{E_S^{\mathcal{G}}(\mathbf{x})}{E^{\mathcal{G}}(\mathbf{x})}, \quad S(\mathbf{X}) = \frac{E_S^{\mathcal{G}}(\mathbf{X})}{E^{\mathcal{G}}(\mathbf{X})} \quad (4)$$

Graph signal with a small S -value means it is a smooth function define on \mathcal{G} . S can be different depends on the Laplacian we use to train GNN and S can be larger than 1. In this paper, we use L_{sym} and \hat{L}_{sym} to measure the smoothness of input features \mathbf{X} and labels \mathbf{y} for different GNNs.

Filterbank GNNs: One Channel to Two

In this section, we state why it is necessary to switch to the two-channel filtering process from only one-channel. Then, we propose the filterbank-GNN framework which can learn a mixture of smooth and non-smooth graph signals.

Motivation

We measure the smoothness of 9 frequently used benchmark datasets and present the results with the network characteristics for each task in Table 1). It shows that the input features and ground truth labels of different datasets are all mixtures of smooth and non-smooth graph signals but in different proportions. Besides, it illustrates that different tasks have different demands of learning how to smoothen the input signals. For example, in *Cora-full*, *Citeseer-full* and *Pubmed-full*, the ground truth labels are much smoother than the input features, such pattern motivates us to learn

how to smoothen the input signals; while in *Wisconsin* and *Texas*, the labels are less smooth than the input features, thus there is no reason that we still learn how to smoothen the input signals. We therefore propose that we should learn both smooth and non-smooth components of the input features instead of merely extracting the smooth part. This motivates us to use filterbanks (LP and HP filters) to filter the signals in GNNs.

LP, HP Graph Filters and Filter Banks The multiplication of L and \mathbf{x} acts as a filtering operation over \mathbf{x} , adjusting the scale of the components of \mathbf{x} in frequency domain. To see this, consider

$$\mathbf{x} = \sum_i u_i u_i^T \mathbf{x}, \quad L \mathbf{x} = \sum_i \lambda_i u_i u_i^T \mathbf{x} \quad (5)$$

The projection $u_i u_i^T \mathbf{x}$ corresponding to a large $|\lambda_i|$ will be amplified, while the one corresponding to a small $|\lambda_i|$ will be suppressed. More specifically, a graph filter that filters out smooth (non-smooth) components is called HP (LP) filter. Generally, the Laplacian matrices ($L_{\text{sym}}, L_{\text{rw}}, \hat{L}_{\text{sym}}, \hat{L}_{\text{rw}}$) can be regarded as HP filters (Ekambaram 2014) and affinity matrices ($A_{\text{sym}}, A_{\text{rw}}, \hat{A}_{\text{sym}}, \hat{A}_{\text{rw}}$) can be treated as LP filters (Maehara 2019). In general, we denote HP and LP filters as L_{HP} and L_{LP} respectively.

On the node level, left multiplying HP and LP filters on \mathbf{x} can be understood as diversification and aggregation operations, respectively. For example, if we implement L_{rw} and A_{rw} on the i -th node, we have

$$(L_{\text{rw}} \mathbf{x})_i = \sum_{j \in N_i} \frac{1}{D_{ii}} (x_i - x_j), \quad (A_{\text{rw}} \mathbf{x})_i = \sum_{j \in N_i} \frac{1}{D_{ii}} x_j \quad (6)$$

Intuitively, HP filters depict the differences between one node and its neighbors, making it distinguishable; While LP filters focus on the similarity within a neighborhood, from which we can obtain missing or ‘‘hidden’’ features of one node. We believe that these two conjugate components are both indispensable to portray a node.

Mathematically, multiplying with LP filter (aggregation) is a linear projection, which means no matter what features we learn, they will be projected to a fixed subspace. We will lose the expressive power by only using LP filter, additionally the missing half is the HP component of the learned signals, as $L_{\text{LP}} + L_{\text{HP}} = I$.

The two-channel linear filterbank which contains a set of filters L_{LP} and L_{HP} is widely used in graph signal processing (Ekambaram et al. 2013; Ekambaram 2014), where L_{LP} and L_{HP} keep the low-frequency and high-frequency components of the graph signals respectively. Inspired by this technique, we propose the two-channel filterbank GNNs that can extract both smooth and non-smooth signals in input features.

Separate Nonlinear Feature Extraction Before Filtering

Before filtering, there is often a learnable linear transformation by parameter matrix, which can be inter-

Table 1: Dataset Overview: Network Characteristics and S -values measured by L_{sym}

datasets		Cornell	Wisconsin	Texas	Actor	Chameleon	Squirrel	Cora-full	Citeseer-full	Pubmed-full
Network Info	#nodes	183	251	183	7600	2277	5201	2708	3327	19717
	#edges	295	499	309	33544	36101	217073	5429	4732	44338
	#features	1703	1703	1703	931	2325	2089	1433	3703	500
	#classes	5	5	5	5	5	5	7	6	3
S-values	input feature	0.904	0.873	0.854	0.901	0.99	0.987	0.862	0.799	0.832
	label	0.883	0.877	0.909	0.836	0.747	0.782	0.288	0.35	0.501
	diff (label - feature)	-0.021	0.004	0.055	-0.065	-0.243	-0.205	-0.574	-0.449	-0.331

We use blue and red shades to demonstrate the relation between label and feature: the label of the blue shaded datasets is smoother than its feature and red datasets are less smooth.

interpreted as, first to learn a shared linear projection for all nodes and then use the predefined filter to select parts of the projection.

For one-channel filtering, there is only one kind of information extracted and sent to the LP filter. While for two-channel filtering, HP and LP filters need to prioritize on the interested information of the layer input in different manners. To make sure the information fed to the two filters are distinctly different and not equivalent after linear transformation, we implement two separate non-linear transformations on the input to excavate the information that each filter needs. This can be easily implemented with, *e.g.*,

$$H^1 = f(\hat{A}_{\text{rw}} \cdot f(XW))$$

Here, f is the activation function. Some one-channel GNNs use similar technique in their architecture designs, *e.g.*, GraphSAINT (Zeng et al. 2019) and GCNII (Chen et al. 2020). This is equivalent to merging a single layer fully connected network (FCN) (Goodfellow, Bengio, and Courville 2016) and a graph filter in one hidden layer, which could also be expected to increase the expressive power. Stronger deep networks, *e.g.*, MLP (Goodfellow, Bengio, and Courville 2016), ResNet (He et al. 2016) and DenseNet (Huang et al. 2017), can also be employed in place of one layer FCN for extraction.

Filter Bank assisted GNNs (FB-GNNs)

Spectral-based FB-GNNs

We use previously defined L_{LP} and L_{HP} to construct the two-channel FB-GNNs as follows (learning framework is provided in figure 1)

$$\mathbf{H}_L^l = L_{\text{LP}} f(\mathbf{H}^{l-1} W_L^{l-1}), \quad \mathbf{H}_H^l = L_{\text{HP}} f(\mathbf{H}^{l-1} W_H^{l-1}) \quad (7)$$

$$\mathbf{H}^l = \alpha_L^l \cdot \mathbf{H}_L^l + \alpha_H^l \cdot \mathbf{H}_H^l, \quad l = 1, \dots, n \quad (8)$$

where $\mathbf{H}^0 = \mathbf{X}$; f is an activation function; $W_L^{l-1}, W_H^{l-1} \in \mathbb{R}^{F_{l-1} \times F_l}$ are learnable parameter matrices focusing on extracting the smooth and non-smooth information from input \mathbf{H}^{l-1} , separately; $\alpha_L^l, \alpha_H^l \in [0, 1]$ are learnable scalar parameters which can learn the relative importance of \mathbf{H}_L^l and \mathbf{H}_H^l and keep a balance between them. In this way, the hidden output \mathbf{H}^l is able to learn a mixture of smooth and non-smooth signals.

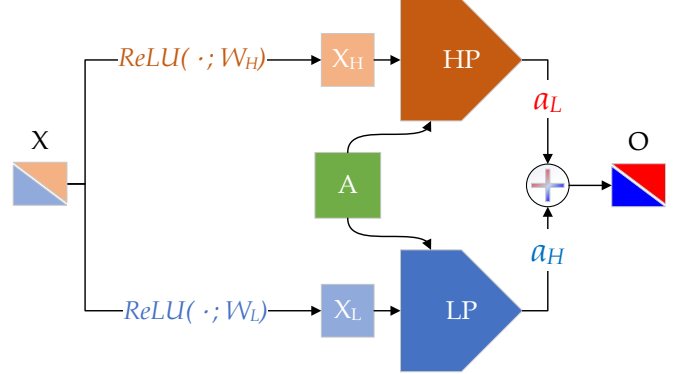


Figure 1: Two-Channel Learning: Information needed for high pass and low pass filters, X_H and X_L , are separately extracted from the input signal X by non-linear transformations. After being filtered by HP and LP, which are both derived upon adjacency matrix A , the filtered signals are again linearly recombined to form the output O .

Spatial-based FB-GNNs

Inspired by (6), the two-channel spatial-based method can be implemented by designing aggregator (LP filter) and diversification operator (HP filter) as follows,

$$\begin{aligned} (\hat{h}_i^l)_L &= f(W_L^{l-1} \mathbf{h}_i^{l-1}), \quad (\hat{h}_i^l)_H = f(W_H^{l-1} \mathbf{h}_i^{l-1}), \\ (\mathbf{h}_i^l)_L &= \sum_{j \in \{\mathcal{N}; \text{Ui}\}} w_{ij} ((\hat{h}_i^l)_L + (\hat{h}_j^l)_L), \\ (\mathbf{h}_i^l)_H &= \sum_{j \in \{\mathcal{N}; \text{Ui}\}} w_{ij} ((\hat{h}_i^l)_H - (\hat{h}_j^l)_H), \quad (9) \\ \mathbf{h}_i^l &= \alpha_L^l \cdot (\mathbf{h}_i^l)_L + \alpha_H^l \cdot (\mathbf{h}_i^l)_H, \quad i = 1, \dots, N, \quad l = 1, \dots, n \end{aligned}$$

where $W_L^{l-1}, W_H^{l-1} \in \mathbb{R}^{F_{l-1} \times F_l}$ are learnable parameter matrices to extract LP and HP features for two channels; w_{ij} is the connection weight between node i and node j , it can be a fixed value or a learnable attention coefficient such as (Velickovic et al. 2017); $\alpha_L^l, \alpha_H^l \in [0, 1]$ are learnable scalar parameters.

Computational Cost: Parameters and Runtime The spectral two-channel learning introduces additionally

one GCN operation and one weighted sum (with negligible costs introduced with non-linearity and weighted sum before output); For spatial methods, similarly, the two-channel learning introduces one additional node-wise subtraction and one additional weighted sum for training on each pair of nodes. Thus, the computational cost and the number of parameters are approximately doubled;

For runtime, overlooking the minor overhead of synchronization, the computations introduced with the additional pass are naturally parallelizable with the original pass (for their independently associated parameters) both in the forward and backward passes. Therefore, no significant additional computational time will be incurred on modern GPU architectures.

Related Works

Dirichlet energy Dirichlet energy (more generally in p -Dirichlet form) is usually used as a regularizer or objective function to impose local neighborhood smoothness in various machine learning tasks, *e.g.*, spectral clustering (Belkin and Niyogi 2002), image processing (Elmoataz, Lezoray, and Bougleux 2008; Bougleux, Elmoataz, and Melkemi 2009; Zheng et al. 2010), non-negative matrix factorization (Cai et al. 2010), matrix completion, principal component analysis (PCA), semi-supervised learning (Zhu, Ghahramani, and Lafferty 2003; Zhu and Lafferty 2005; Belkin, Niyogi, and Sindhwani 2006). It has different names in different literature, *e.g.*, Laplacian regularizer (Zheng et al. 2010), manifold regularizer (Cai et al. 2010), quadratic energy function (Zhu, Ghahramani, and Lafferty 2003), *etc.*

Instead of using Dirichlet energy in training process, we point out that combining with graph signal energy, it can be used to measure the smoothness of the input features and output labels for a given learning task. With this, the necessity of learning the non-smoothness component can be confirmed.

Measuring Smoothness The authors of (Pei et al. 2020) propose a method to measure the smoothness (homophily) of ground truth labels of dataset as follows,

$$\frac{1}{|\mathcal{V}|} \sum_{v \in \mathcal{V}} \frac{\#v \text{ 's neighbors who have the same label as } v}{\#v \text{ 's neighbors}}$$

(Zhu et al. 2020) proposes edge homophily ratio, which is the fraction of edges that the connected nodes share the same label (*i.e.*, intra-class edges). Both of these methods do not provide an extension definition on block matrix. Thus, they fail to measure the smoothness of the input features and cannot be used to compare the difference of smoothness between the input features and labels.

On Addressing Heterophily Geom-GCN (Pei et al. 2020) uses a geometric aggregation scheme and a bi-

level aggregator to capture the information of structural neighborhoods, which can be distant nodes. These can efficiently take use of the geometric relationships defined in the latent space. H₂GCN (Zhu et al. 2020) designs ego- and neighbor-embedding separation, aggregation of higher-order neighborhoods, and combination of intermediate representations to generalize the limitation of existing GNNs beyond homophily setting. Non-local GNNs (Liu, Wang, and Ji 2020) propose a simple and effective non-local aggregation framework with an efficient attention-guided sorting for GNNs.

The aforementioned works design various tricks, trying to take use of multi-hop neighborhood information and capture long-range dependencies with the belief that heterophily problem could be alleviated with the help of the distant nodes. Although these methods show some promising results, the effectiveness is limited and do not jump out of the scope of neighborhood aggregation. In this paper, We target directly its cause, handling heterophily problem by seeking the distinctiveness between nodes with an additional channel to learn the non-smoothness components.

Experiments

In this section, we first validate whether the two-channel filtering and learning procedure lead to better representation learning when patched on popular shallow GNN baselines²: GraphSAINT (Zeng et al. 2019), GraphSAGE (Hamilton, Ying, and Leskovec 2017), Graph Attention Network (GAT) (Velickovic et al. 2017), GCN (Kipf and Welling 2016), Geom-GCN-P (-S and -I) (Pei et al. 2020) and Graph Wavelet Neural Network (GWNN) (Xu et al. 2019). Deeper GNNs are shown to have the potentials of mitigating the heterophily problem by extracting multi-hop neighborhood information. For them, we test the two-channel framework on two state-of-the-art methods GCNII and GCNII* (Chen et al. 2020), with varied model depths. After these, we validate the effectiveness of each proposed component with a detailed ablation test.

The experiments are conducted in the form of node classification under supervised learning setting and performed on 9 datasets including *Cornell*, *Wisconsin*, *Texas*, *Actor*, *Chameleon*, *Squirrel*, *Cora*, *Citeseer*, and *Pubmed* (details to be found in the appendix). Their rough characteristics are shown in Table 1.

Experimental Setup

In supervised learning of shallow GNNs, we keep the same training configurations for GraphSAINT and FB-GraphSAINT on the 9 datasets, which are the random walk sampler with length 2 (RW) setting³ in GraphSAINT (Zeng et al. 2019); for GWNN (Xu et al. 2019)

²Source code submitted within supplementary materials and to be published after the review.

³The name “random walk sampler with length 2 setting” is what the authors used in their paper and they use the name *PPI-large-2* in their code.

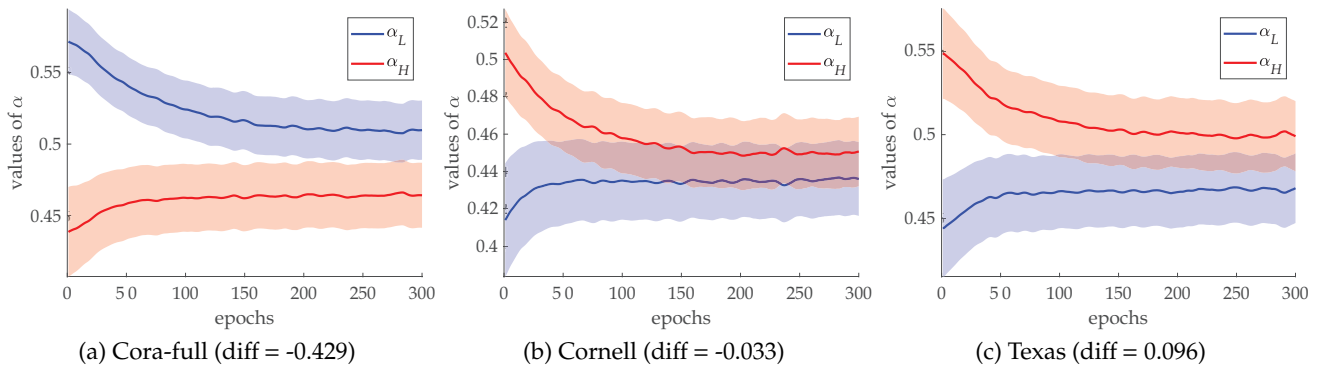


Figure 2: α_L and α_H in the output layer of FB-GraphSAINT trained on Cora-full, Cornell and Texas. The mean curves and the std bands are obtained over 20 independent runs. See diff values in table 3.

and FB-GWNN, we use the same hyperparameters $s = 1.0, t = 10^{-4}$ on the 9 datasets⁴. Other GNNs and their two-channel variants are under the same experiment settings as (Hamilton, Ying, and Leskovec 2017) and (Pei et al. 2020).

For supervised learning on deep GNNs, GCNII, GCNII*, FB-GCNII, and FB-GCNII* use $\lambda = 1.5$ and $\alpha = 0.2$ on *Actor* and *Squirrel*. Other deep models use the same training configurations as GCNII (Chen et al. 2020) on the remaining 7 datasets.

For all experiments, we randomly split the nodes of each class into 60%/ 20%/ 20% for training, validation and testing as suggested in (Pei et al. 2020). We report the average performance of all models on the test sets over 10 random splits⁵.

Supervised Learning of Shallow GNNs

In Table 2, we summarize the mean accuracy of shallow baseline GNNs and their filterbank versions. The best performance is highlighted. Also, we record the performance differences between baselines and the two-channel augmented methods in the brackets. From the results we can see that, our propose methods generally boost the performance of almost all cases, especially when the labels are not much smoother than the input features indicated, considering the S -values in Table 3.

Table 3 shows that the S -values of FB-GCN outputs are closer to the S -values of the ground truth labels (see the absolute differences in the bracket) compared with those of GCN outputs. This indicates that FB-GCN is able to learn better representations which can reconstruct both the smooth and non-smooth part of the ground truth labels. Note that we measure the smoothness by \hat{L}_{sym} instead of L_{sym} , because GCN is train with

⁴This set of hyperparameters is the same as that of the original paper when training GWNN on Cora.

⁵We obtain the performance of GAT, GCN, and GEOM-GCN-P(-S and -I) directly from (Pei et al. 2020); and we reproduce other baseline models and implement all the filterbank GNNs.

renormalized affinity matrix \hat{A}_{sym} .

Supervised Learning of Deep GNNs

In this subsection, we build deep multi-hop filterbank models based on the architecture of GCNII and GCNII* (Chen et al. 2020) to see if the two-channel method is capable to assist deep GNN models. We report mean accuracy, highlight best performing depth, and record performance difference in brackets in Table 5. In general, FB-GCNII and FB-GCNII* achieve better results than the unpatched GCNII and GCNII* at different depths, especially on *Wisconsin* and *Texas*, where the non-smooth part of representations are desirable.

Ablation Tests

In this subsection, we perform ablation tests by using FB-GraphSAINT (Zeng et al. 2019) on *Cora-full*, *Cornell* and *Texas* accordingly, which are the three principally different datasets measured by \hat{L}_{sym} in Table 3. The ablation tests would examine the effectiveness of each proposed component. The results are summarized in Table 6. The results show that both the non-linear feature extractor and two-path filters are able to help capture richer information. And they two together can assist each other and achieve better performance.

Moreover, to emphasize the importance of HP component, we also show the learnable coefficients α_L and α_H for two components on FB-GraphSAINT over the 9 datasets at the validation stage in Table 4. For most of the tasks, neither the coefficients for LP nor HP are negligible. Among 6 out of 9 tasks, the learned coefficients for the HP components are even greater, this indicates the necessity of the HP components in graph representation learning.

In addition, Figure 2 shows the averaged real-time change of the learned coefficients α_L and α_H in the output layer of FB-GraphSAINT on *Cora-full*, *Cornell* and *Texas* during training. We can see that α_L and α_H will converge to a pair of values that explains how the smooth and non-smooth features will be mixed. The

Table 2: Supervised Learning of Shallow GNNs

Models/Datasets	Cornell	Wisconsin	Texas	Actor	Chameleon	Squirrel	Cora-full	Citeseer-full	Pubmed-full
Diff of S-values	-0.021	0.004	0.055	-0.065	-0.243	-0.205	-0.574	-0.449	-0.330
Spatial Methods(%)									
GraphSAINT	70.27	71.35	72.97	17.89	43.86	33.27	84.69	73.2	89.42
FB-GraphSAINT	78.38(8.11)	80(8.65)	75.68(2.71)	19.08(1.19)	46.05(2.19)	36.06(2.79)	87.5(2.81)	74.76(1.56)	89.88(0.46)
GraphSAGE	54.05	66	56.76	14.67	40.13	24.14	80.64	72.36	85.49
FB-GraphSAGE	63.14(9.09)	70(4)	58.05(1.29)	23.27(8.6)	39.74(-0.39)	24.6(0.46)	83.7(3.06)	72.58(0.22)	86.31(0.82)
Spectral Methods(%)									
GAT	54.32	49.41	58.38	28.45	42.93	30.03	86.37	74.32	87.62
FB-GAT	64.86(10.54)	60.78(11.37)	64.86(6.48)	30.66(2.21)	47.37(4.44)	31.8(1.77)	88.73(2.36)	77.12(2.8)	88.16(0.54)
GCN	52.7	45.88	52.16	26.86	28.18	23.96	85.77	73.68	88.13
FB-GCN	62.16(9.46)	56.86(10.98)	62.16(10.00)	31.21(4.35)	32.89(4.71)	24.73(0.77)	85.92(0.15)	75.24(1.56)	88.54(0.41)
Geom-GCN-P	60.81	64.12	67.57	31.63	60.9	38.14	84.93	75.14	88.09
FB-Geom-GCN-P	64.86(4.05)	72.55(8.43)	70.27(2.70)	31.02(-0.61)	67.20(6.30)	49.66(11.52)	85.17(0.24)	76.23(1.09)	88.25(0.16)
Geom-GCN-S	55.68	56.67	59.73	30.3	59.96	36.24	85.27	74.71	84.75
FB-Geom-GCN-S	56.54(0.86)	56.94(0.27)	62.16(2.43)	31.25(0.95)	61.49(1.53)	37.27(1.03)	85.43(0.16)	75.21(0.5)	85.88(1.13)
Geom-GCN-I	56.76	58.24	57.58	29.09	60.31	33.32	85.19	77.99	90.05
FB-Geom-GCN-I	57.38(0.62)	60.68(2.44)	62.21(4.63)	31.45(2.36)	60.76(0.45)	35.27(1.95)	85.45(0.26)	77.69(-0.3)	90.48(0.43)
GWNN	70.67	72.22	69.44	20.92	33.63	29.13	84.49	72.47	83.6
FB-FWNN	80.11(9.44)	84.67(12.45)	77.78(8.34)	22.24(1.32)	37.36(3.73)	30.6(1.47)	85.6(1.11)	72.83(0.36)	85.92(2.32)
Baseline Average	59.41	60.49	62.32	26.2	46.46	31.44	85.15	74.33	87.3
FB-Baseline Average	65.93(6.52)	67.81(7.32)	66.65(4.33)	27.52(1.32)	49.11(2.65)	33.75(2.31)	85.94(1.27)	75.21(0.97)	87.93(0.63)

The results are averaged from 10 independent runs. The (values) represent the difference of performance brought by patching FB.

Table 3: Statistics of Datasets (measured by \hat{L}_{sym} instead of L_{sym}) and Comparison of the Output Smoothness

datasets	Cornell	Wisconsin	Texas	Actor	Chameleon	Squirrel	Cora-full	Citeseer-full	Pubmed-full
input feature	0.172	0.385	0.205	0.567	0.831	0.87	0.617	0.515	0.529
label	0.139	0.328	0.301	0.511	0.638	0.681	0.188	0.209	0.272
S-values diff (label - feature)	-0.033	-0.057	0.096	-0.056	-0.193	-0.189	-0.429	-0.306	-0.257
GCN output	0.037 (0.102)	0.124 (0.204)	0.139 (0.162)	0.397 (0.114)	0.595 (0.043)	0.578 (0.103)	0.156 (0.032)	0.112 (0.097)	0.234 (0.038)
FB-GCN output	0.099 (0.040)	0.269 (0.059)	0.201 (0.100)	0.531 (0.020)	0.655 (0.017)	0.683 (0.002)	0.172 (0.016)	0.148 (0.061)	0.247 (0.025)

These results are obtained from 10 independent runs. The stds are negligible so they are not presented (mostly < 0.002). This table shows how FB-patched baseline could better reconstruct the label smoothness, *i.e.* we want the S-value of the output to be closer to that of the labels. The (values) stand for the absolute difference between the S-values of the output of the methods and those of the ground truths. Better reconstruction between the two methods on each task is marked **bold**.

Table 4: α_L and α_H in the Output Layer of FB-GraphSAINT

	Cornell	Wisconsin	Texas	Actor	Chameleon	Squirrel	Cora-full	Citeseer-full	Pubmed-full
α_L	0.436	0.441	0.57	0.54	0.701	0.675	0.509	0.514	0.473
α_H	0.45	0.499	0.6	0.557	0.713	0.65	0.464	0.503	0.478
α_H/α_L	1.032	1.132	1.053	1.031	1.017	0.963	0.912	0.979	1.011

The results are averaged from 10 independent runs. If the ratio is higher than 1.0, then the high frequency signals are more important. The higher the ratio, the more important HP filter is.

Table 5: Supervised Learning of Deep Multi-scale GNNs

Models\Datasets	Cornell	Wisconsin	Texas	Actor	Chameleon	Squirrel	Cora-full	Citeseer-full	Pubmed-full
GCNII-8	70.54	73.88	71.08	33.7	60.61	37.49	85.69	75.54	88.62
FB-GCNII-8	75.95(5.41)	82.35(8.47)	74.59(3.51)	35.37(1.67)	60.43(-0.18)	39.69(2.2)	86.04(0.35)	75.51(-0.03)	89.97(1.35)
GCNII-16	74.86	74.12	69.46	33.62	55.48	35.98	87.3	76.54	88.28
FB-GCNII-16	77.57(2.71)	82.55(8.43)	77.03(7.57)	35.12(1.5)	56.78(1.3)	39.38(3.4)	87.5(0.2)	76.67(0.13)	89.39(1.11)
GCNII-32	72.7	70.2	69.46	31.61	53.71	35.92	88.13	76.08	87.89
FB-GCNII-32	72.81(0.11)	78.63(8.43)	80.27(10.81)	32.99(1.38)	54.98(1.27)	36.81(0.89)	88.33(0.2)	76.49(0.41)	89.1(1.21)
GCNII-64	71.89	68.84	66.49	28.76	54.14	36.1	88.49	77.08	89.57
FB-GCNII-64	76.49(4.6)	76.27(7.43)	76.22(9.73)	29.57(0.81)	54.39(0.25)	36.79(0.69)	87.92(-0.57)	77(-0.08)	89.65(0.08)
GCNII*-8	72.97	78.82	72.7	34.89	62.48	40.72	86.14	75.06	89.7
FB-GCNII*-8	76.76(3.79)	82.94(4.12)	78.11(5.41)	35.87(0.98)	65.11(2.63)	41.19(0.47)	86.94(0.8)	76.32(1.26)	90.2(0.5)
GCNII*-16	76.49	81.57	75.41	34.18	58.86	39.88	87.46	75.8	86.69
FB-GCNII*-16	76.95(0.46)	82.39(0.82)	76.76(1.35)	35.4(1.22)	59.98(1.12)	40.08(0.2)	87.48(0.02)	76.43(0.63)	89.95(3.26)
GCNII*-32	74.32	77.06	77.84	33.78	56.27	37.69	88.35	76.55	89.37
FB-GCNII*-32	74.51(0.19)	80.78(3.72)	84.86(7.02)	34.73(0.95)	57.65(1.38)	41.24(3.55)	88.16(-0.19)	76.89(0.34)	89.92(0.55)
GCNII*-64	72.43	73.53	75.41	32.72	53.82	36.83	88.01	77.13	90.3
FB-GCNII*-64	75.84(3.41)	81.57(8.04)	80.54(5.13)	34.89(2.17)	57.52(3.7)	39.81(2.98)	87.44(-0.57)	77.03(-0.1)	89.98(-0.32)
Baseline Average	73.28	74.75	72.23	32.91	56.92	37.58	87.45	76.22	88.8
FB-Baseline Average	75.86(2.58)	80.94(6.19)	78.55(6.32)	34.24(1.33)	58.36(1.44)	39.37(1.79)	87.48(0.03)	76.54(0.32)	89.77(0.97)

The results are averaged from 10 independent runs. The (values) represent the difference of performance brought by patching FB.

Table 6: Ablation Results: Accuracy (%)

#ch	transform	Cora-full		Cornell		Texas	
		mean	std	mean	std	mean	std
1	linear	83.92	1.0	64.86	2.2	70.60	1.9
1	nonlinear	84.69	0.5	70.27	0.8	72.97	0.8
2	linear	85.02	2.1	75.64	2.0	74.15	2.1
2	nonlinear	87.50	1.6	78.38	1.5	75.68	1.0

Color indicators are added to differentiate the performance of each test case: the greener the better, the redder the worse

fact that the ratio α_H/α_L is close to 1 again shows that the importance of the non-smooth part in constructing the output signal. More specifically, the importance (red line) is higher when the demand of non-smooth outputs (diff values) is higher.

Conclusion

This paper recognizes the role of high-frequency information in graph representation learning. The proposed HP filter completes the spectrum of graph filters and yield significant better representation learning on several empirical tasks.

References

- Belkin, M.; and Niyogi, P. 2002. Laplacian eigenmaps and spectral techniques for embedding and clustering. In *Advances in neural information processing systems*, 585–591.
- Belkin, M.; Niyogi, P.; and Sindhwani, V. 2006. Manifold regularization: A geometric framework for learning from labeled and unlabeled examples. *Journal of machine learning research* 7(Nov): 2399–2434.
- Bougleux, S.; Elmoataz, A.; and Melkemi, M. 2009. Local and nonlocal discrete regularization on weighted graphs for image and mesh processing. *International journal of computer vision* 84(2): 220–236.
- Bronstein, M. M.; Bruna, J.; LeCun, Y.; Szlam, A.; and Vandergheynst, P. 2016. Geometric deep learning: going beyond Euclidean data. *arXiv abs/1611.08097*. URL <http://arxiv.org/abs/1611.08097>.
- Bruna, J.; Zaremba, W.; Szlam, A.; and LeCun, Y. 2014. Spectral Networks and Locally Connected Networks on Graphs. *arXiv abs/1312.6203*. URL <http://arxiv.org/abs/1312.6203>.
- Cai, D.; He, X.; Han, J.; and Huang, T. S. 2010. Graph regularized nonnegative matrix factorization for data representation. *IEEE transactions on pattern analysis and machine intelligence* 33(8): 1548–1560.
- Cai, D.; Wang, X.; and He, X. 2009. Probabilistic dyadic data analysis with local and global consistency. In *Proceedings of the 26th annual international conference on machine learning*, 105–112.
- Chen, M.; Wei, Z.; Huang, Z.; Ding, B.; and Li, Y. 2020. Simple and Deep Graph Convolutional Networks. *arXiv preprint arXiv:2007.02133*.
- Chung, F. R.; and Graham, F. C. 1997. *Spectral graph theory*. 92. American Mathematical Soc.
- Daković, M.; Stanković, L.; and Sejdić, E. 2019. Local smoothness of graph signals. *Mathematical Problems in Engineering* 2019.
- Defferrard, M.; Bresson, X.; and Vandergheynst, P. 2016. Convolutional Neural Networks on Graphs with Fast Localized Spectral Filtering. *arXiv abs/1606.09375*. URL <http://arxiv.org/abs/1606.09375>.
- Ekambaram, V. N. 2014. *Graph structured data viewed through a fourier lens*. University of California, Berkeley.
- Ekambaram, V. N.; Fanti, G.; Ayazifar, B.; and Ramchandran, K. 2013. Critically-sampled perfect-reconstruction spline-wavelet filterbanks for graph signals. In *2013 IEEE Global Conference on Signal and Information Processing*, 475–478. IEEE.
- Elmoataz, A.; Lezoray, O.; and Bougleux, S. 2008. Non-local discrete regularization on weighted graphs: a framework for image and manifold processing. *IEEE transactions on Image Processing* 17(7): 1047–1060.
- Evans, L. C. 1998. Partial differential equations. Graduate studies in mathematics. *American mathematical society* 2: 1998.
- Gavili, A.; and Zhang, X.-P. 2017. On the shift operator, graph frequency, and optimal filtering in graph signal processing. *IEEE Transactions on Signal Processing* 65(23): 6303–6318.
- Gilmer, J.; Schoenholz, S. S.; Riley, P. F.; Vinyals, O.; and Dahl, G. E. 2017. Neural message passing for quantum chemistry. In *Proceedings of the 34th International Conference on Machine Learning-Volume 70*, 1263–1272. JMLR.org.
- Goodfellow, I.; Bengio, Y.; and Courville, A. 2016. *Deep learning*. MIT press.
- Hamilton, W. L.; Ying, R.; and Leskovec, J. 2017. Inductive Representation Learning on Large Graphs. *arXiv abs/1706.02216*. URL <http://arxiv.org/abs/1706.02216>.
- He, K.; Zhang, X.; Ren, S.; and Sun, J. 2016. Deep residual learning for image recognition. In *Proceedings of the IEEE conference on computer vision and pattern recognition*, 770–778.
- He, X.; and Niyogi, P. 2004. Locality preserving projections. In *Advances in neural information processing systems*, 153–160.
- Huang, G.; Liu, Z.; Van Der Maaten, L.; and Weinberger, K. Q. 2017. Densely connected convolutional networks. In *Proceedings of the IEEE conference on computer vision and pattern recognition*, 4700–4708.
- Jiang, Y.; Bolnick, D. I.; and Kirkpatrick, M. 2013. Assortative mating in animals. *The American Naturalist* 181(6): E125–E138.
- Kalofolias, V. 2016. How to learn a graph from smooth signals. In *Artificial Intelligence and Statistics*, 920–929.
- Kipf, T. N.; and Welling, M. 2016. Semi-Supervised Classification with Graph Convolutional Networks. *arXiv abs/1609.02907*. URL <http://arxiv.org/abs/1609.02907>.
- LeCun, Y.; Bengio, Y.; and Hinton, G. 2015. Deep learning. *nature* 521(7553): 436.
- LeCun, Y.; Bottou, L.; Bengio, Y.; Haffner, P.; et al. 1998. Gradient-based learning applied to document recognition. *Proceedings of the IEEE* 86(11): 2278–2324.
- Liao, R.; Zhao, Z.; Urtasun, R.; and Zemel, R. S. 2019. LanczosNet: Multi-Scale Deep Graph Convolutional Networks. *arXiv abs/1901.01484*. URL <http://arxiv.org/abs/1901.01484>.
- Liu, M.; Wang, Z.; and Ji, S. 2020. Non-Local Graph Neural Networks. *arXiv preprint arXiv:2005.14612*.
- Luan, S.; Zhao, M.; Chang, X.-W.; and Precup, D. 2019. Break the Ceiling: Stronger Multi-scale Deep Graph Convolutional Networks. *arXiv preprint arXiv:1906.02174*.
- Maehara, T. 2019. Revisiting Graph Neural Networks: All We Have is Low-Pass Filters. *arXiv preprint arXiv:1905.09550*.

- McPherson, M.; Smith-Lovin, L.; and Cook, J. M. 2001. Birds of a feather: Homophily in social networks. *Annual review of sociology* 27(1): 415–444.
- Monti, F.; Boscaini, D.; Masci, J.; Rodola, E.; Svoboda, J.; and Bronstein, M. M. 2017. Geometric deep learning on graphs and manifolds using mixture model cnns. In *Proceedings of the IEEE Conference on Computer Vision and Pattern Recognition*, 5115–5124.
- Newman, M. E. 2003. Mixing patterns in networks. *Physical review E* 67(2): 026126.
- Pandit, S.; Chau, D. H.; Wang, S.; and Faloutsos, C. 2007. Netprobe: a fast and scalable system for fraud detection in online auction networks. In *Proceedings of the 16th international conference on World Wide Web*, 201–210.
- Pei, H.; Wei, B.; Chang, K. C.-C.; Lei, Y.; and Yang, B. 2020. Geom-gcn: Geometric graph convolutional networks. *arXiv preprint arXiv:2002.05287* .
- Rogers, E. M. 2010. *Diffusion of innovations*. Simon and Schuster.
- Rozemberczki, B.; Allen, C.; and Sarkar, R. 2019. Multi-scale Attributed Node Embedding.
- Sen, P.; Namata, G. M.; Bilgic, M.; Getoor, L.; Gallagher, B.; and Eliassi-Rad, T. 2008. Collective Classification in Network Data. *AI Magazine* 29(3): 93–106. URL <http://www.cs.iit.edu/~ml/pdfs/sen-aimag08.pdf>.
- Shuman, D. I.; Narang, S. K.; Frossard, P.; Ortega, A.; and Vandergheynst, P. 2013. The emerging field of signal processing on graphs: Extending high-dimensional data analysis to networks and other irregular domains. *IEEE signal processing magazine* 30(3): 83–98.
- Smith, K.; Spyrou, L.; and Escudero, J. 2018. Graph-variate signal analysis. *IEEE Transactions on Signal Processing* 67(2): 293–305.
- Stanković, L.; Sejdić, E.; and Daković, M. 2018. Reduced interference vertex-frequency distributions. *IEEE Signal Processing Letters* 25(9): 1393–1397.
- Velickovic, P.; Cucurull, G.; Casanova, A.; Romero, A.; Lio, P.; and Bengio, Y. 2017. Graph attention networks. *arXiv abs/1710.10903*.
- Wu, F.; Zhang, T.; Souza Jr, A. H. d.; Fifty, C.; Yu, T.; and Weinberger, K. Q. 2019a. Simplifying graph convolutional networks. *arXiv preprint arXiv:1902.07153* .
- Wu, Z.; Pan, S.; Chen, F.; Long, G.; Zhang, C.; and Yu, P. S. 2019b. A Comprehensive Survey on Graph Neural Networks. *arXiv abs/1901.00596*. URL <http://arxiv.org/abs/1901.00596>.
- Xu, B.; Shen, H.; Cao, Q.; Qiu, Y.; and Cheng, X. 2019. Graph Wavelet Neural Network. *arXiv preprint arXiv:1904.07785* .
- Zeng, H.; Zhou, H.; Srivastava, A.; Kannan, R.; and Prasanna, V. 2019. Graphsaint: Graph sampling based inductive learning method. *arXiv preprint arXiv:1907.04931* .
- Zhang, S.; Tong, H.; Xu, J.; and Maciejewski, R. 2019. Graph convolutional networks: a comprehensive review. *Computational Social Networks* 6(1): 11.
- Zheng, M.; Bu, J.; Chen, C.; Wang, C.; Zhang, L.; Qiu, G.; and Cai, D. 2010. Graph regularized sparse coding for image representation. *IEEE transactions on image processing* 20(5): 1327–1336.
- Zhou, D.; Bousquet, O.; Lal, T. N.; Weston, J.; and Schölkopf, B. 2004. Learning with local and global consistency. In *Advances in neural information processing systems*, 321–328.
- Zhu, J.; Yan, Y.; Zhao, L.; Heimann, M.; Akoglu, L.; and Koutra, D. 2020. Generalizing Graph Neural Networks Beyond Homophily. *arXiv preprint arXiv:2006.11468* .
- Zhu, X.; Ghahramani, Z.; and Lafferty, J. D. 2003. Semi-supervised learning using gaussian fields and harmonic functions. In *Proceedings of the 20th International conference on Machine learning (ICML-03)*, 912–919.
- Zhu, X.; and Lafferty, J. 2005. Harmonic mixtures: combining mixture models and graph-based methods for inductive and scalable semi-supervised learning. In *Proceedings of the 22nd international conference on Machine learning*, 1052–1059.

Dataset Descriptions

For node classification, there are 4 main categories:

Cora, *Citeseer*, and *Pubmed* are 3 benchmark datasets (Sen et al. 2008) in the category of *Citation network*. Such networks use nodes to represent papers and edges to denote citations. Node features are the bag-of-words representation and node labels are classified into different academic topics.

Cornell, *Texas*, and *Wisconsin* belong to the webpage dataset *WebKB* (Pei et al. 2020) created by Carnegie Mellon University. Each node represents a web page, and the edges are hyperlinks between nodes. Node features are the bag-of-words representation and node labels are in five classes.

Chameleon and *Squirrel* are two page-to-page networks in the *Wikipedia network* (Rozemberczki, Allen, and Sarkar 2019). Nodes represent web pages and edges show mutual links between pages. Node features are informative nouns in the Wikipedia pages and nodes are classified into 5 groups based on monthly views.

Actor refers to the *Actor co-occurrence network*. A node corresponds to an actor, and an edge exists if two actors occur on the same Wikipedia page. Node features correspond to some keywords in the Wikipedia pages, and nodes are categorized into five classes of words of actors' Wikipedia.